Otterbein University
Digital Commons @ Otterbein

Biology and Earth Science Faculty Scholarship | Biology and Earth Science

2-23-2016

Distinct Components of Retrograde CaV1.1-RyR1 Coupling Revealed by a Lethal Mutation in RyR1

David Sheridan
Otterbein University

Follow this and additional works at: https://digitalcommons.otterbein.edu/bio_fac

 Part of the Biology Commons

Repository Citation

Sheridan, David, "Distinct Components of Retrograde CaV1.1-RyR1 Coupling Revealed by a Lethal Mutation in RyR1" (2016). *Biology and Earth Science Faculty Scholarship*. 22.
https://digitalcommons.otterbein.edu/bio_fac/22

This Article is brought to you for free and open access by the Biology and Earth Science at Digital Commons @ Otterbein. It has been accepted for inclusion in Biology and Earth Science Faculty Scholarship by an authorized administrator of Digital Commons @ Otterbein. For more information, please contact digitalcommons07@otterbein.edu.

Article

Distinct Components of Retrograde $Ca_V1.1$-RyR1 Coupling Revealed by a Lethal Mutation in RyR1

Roger A. Bannister,[1,*] David C. Sheridan,[2] and Kurt G. Beam[3,*]
[1]Cardiology Division, Department of Medicine, University of Colorado School of Medicine, Aurora, Colorado; [2]Department of Biology and Earth Science, Otterbein University, Westerville, Ohio; and [3]Department of Physiology and Biophysics, University of Colorado School of Medicine, Aurora, Colorado

ABSTRACT The molecular basis for excitation-contraction coupling in skeletal muscle is generally thought to involve conformational coupling between the L-type voltage-gated Ca^{2+} channel ($Ca_V1.1$) and the type 1 ryanodine receptor (RyR1). This coupling is bidirectional; in addition to the orthograde signal from $Ca_V1.1$ to RyR1 that triggers Ca^{2+} release from the sarcoplasmic reticulum, retrograde signaling from RyR1 to $Ca_V1.1$ results in increased amplitude and slowed activation kinetics of macroscopic L-type Ca^{2+} current. Orthograde coupling was previously shown to be ablated by a glycine for glutamate substitution at RyR1 position 4242. In this study, we investigated whether the RyR1-E4242G mutation affects retrograde coupling. L-type current in myotubes homozygous for RyR1-E4242G was substantially reduced in amplitude (~80%) relative to that observed in myotubes from normal control (wild-type and/or heterozygous) myotubes. Analysis of intramembrane gating charge movements and ionic tail current amplitudes indicated that the reduction in current amplitude during step depolarizations was a consequence of both decreased $Ca_V1.1$ membrane expression (~50%) and reduced channel P_o (~55%). In contrast, activation kinetics of the L-type current in RyR1-E4242G myotubes resembled those of normal myotubes, unlike *dyspedic* (RyR1 null) myotubes in which the L-type currents have markedly accelerated activation kinetics. Exogenous expression of wild-type RyR1 partially restored L-type current density. From these observations, we conclude that mutating residue E4242 affects RyR1 structures critical for retrograde communication with $Ca_V1.1$. Moreover, we propose that retrograde coupling has two distinct and separable components that are dependent on different structural elements of RyR1.

INTRODUCTION

In skeletal muscle, conformational coupling between the L-type voltage-gated Ca^{2+} channel ($Ca_V1.1$) and the type 1 ryanodine receptor (RyR1) appears to be responsible for the release of Ca^{2+} from the sarcoplasmic reticulum in response to depolarization of the plasma membrane, resulting in the activation of the contractile filaments (1–4). Twenty years ago, Nakai et al. (5) established that in addition to this orthograde signal transmitted from $Ca_V1.1$ to RyR1, there was also a retrograde signal from RyR1 to $Ca_V1.1$. Specifically, examination of L-type Ca^{2+} currents in myotubes harvested from *dyspedic* (RyR1 null) mice revealed that $Ca_V1.1$ channel open probability (P_o) was greatly reduced, implying that the presence of RyR1 somehow increases $Ca_V1.1$ P_o (5–8). Subsequent studies have shown that RyR1 also has a profound impact on $Ca_V1.1$ activation kinetics, as L-type currents in *dyspedic* myotubes display accelerated activation in comparison to those of normal myotubes or *dyspedic* myotubes transfected with wild-type RyR1 (8–10). In addition, $Ca_V1.1$ gating is directly impacted by ryanodine-induced conformational changes in RyR1 (11,12).

There has been extensive work to identify regions of $Ca_V1.1$ and its auxiliary β_{1a} subunit, which are important for bidirectional coupling with RyR1 (13), with the result that the nonconserved sequences of both that are important for this signaling have been somewhat well defined (14–18). Similarly, there have been a number of studies attempting to identify regions of RyR1 important for bidirectional signaling; these have employed both traditional biochemical methods (19–22), and expression of RyR1/RyR2 or RyR1/RyR3 chimeras in *dyspedic* myotubes (6,10,23–26). These studies have provided some information on regions of primary sequence within the myoplasmic foot domain of RyR1 that affect conformational coupling. However, these studies were carried out largely in the absence of information about the three-dimensional arrangement of the primary sequence, and the regions of RyR1 found to be important were relatively large. Thus, much less is known about the structures of RyR1 involved in coupling to $Ca_V1.1$, particularly those involved in retrograde coupling.

Recently, a mutant mouse strain carrying a recessively inherited defect in RyR1 was generated (27). Pups homozygous for this mutation (RyR1-E4242G) died perinatally from asphyxiation and displayed gross morphology similar

Submitted November 16, 2015, and accepted for publication December 30, 2015.

*Correspondence: roger.bannnister@ucdenver.edu or kurt.beam@ucdenver.edu

Editor: Michael Pusch.

© 2016 by the Biophysical Society

0006-3495/16/02/0912/10

http://dx.doi.org/10.1016/j.bpj.2015.12.031

to that of the four existing excitation-contraction (EC) coupling-defective model mouse strains (*dysgenic*, *dyspedic*, β_1 null, and Stac3 null). Myotubes cultured from these homozygous mutant mice (hereafter referred to as RyR1-E4242G) were incapable of supporting depolarization-induced myoplasmic Ca^{2+} transients and electrically evoked contractions; these latter observations made in our laboratory indicated that mutation ablated orthograde $Ca_V1.1$-RyR1 coupling.

The purpose of this study was to investigate whether retrograde coupling is also disrupted by the RyR1-E4242G mutation. Our results indicate that the RyR1-E4242G mutation markedly reduces L-type current density, $Ca_V1.1$ P_o, and $Ca_V1.1$ expression, where this last effect is most likely a consequence of the absence of EC coupling (see Avila et al. (28)). The effects of the RyR1-E4242G mutation on current density, relative P_o, and channel expression are similar to those occurring in *dyspedic* myotubes in which RyR1 has been genetically ablated (5). However, L-type currents of myotubes homozygous for RyR1-E4242G retained the slow activation kinetics characteristic of normal myotubes. As a result of these observations, we conclude that the two components that have been described earlier for retrograde coupling, increased P_o and slowed activation, are in fact separable. Thus, we propose that these two physiological effects rely on different structural elements of RyR1.

MATERIALS AND METHODS

Myotube culture

All procedures involving mice were approved by the University of Colorado Denver-Anschutz Medical Campus Institutional Animal Care and Use Committee. Primary cultures of phenotypically normal (+/+ or +/RyR1^{AG}), RyR1-E4242G homozygous (RyR1^{AG}/RyR1^{AG}), and *dyspedic* (RyR1^{-}/RyR1^{-}) myotubes were prepared from E18.5 mice as described previously in Beam and Franzini-Armstrong (29). Like *dyspedic* mice, RyR1-E4242G mice died from respiratory failure upon parturition (27). Myoblasts were plated into 35 mm ECL-coated, plastic culture dishes (Falcon, Corning, NY). Cultures were grown for 6–7 days in a humidified 37°C incubator with 5% CO_2 in Dulbecco's Modified Eagle Medium (Mediatech, Tewksbury, MA), supplemented with 10% fetal bovine serum/10% horse serum (Hyclone Laboratories, Logan, UT). This medium was then replaced with differentiation medium (Dulbecco's Modified Eagle Medium supplemented with 2% horse serum). For electrophysiological experiments, myotubes were examined 4–6 days postdifferentiation. In some cases, single nuclei of RyR1-E4242G myotubes were microinjected with a solution of plasmid cDNA encoding an RyR1-YFP fusion construct (500 ng/μL; see below) two days postdifferentiation and four days before experiments. Data were obtained from 4 and 10 independent cultures of normal and RyR1-E4242G homozygous myotubes, respectively.

Ca^{2+} current recordings

Pipettes were fabricated from borosilicate glass and had resistances of ~2.0 MΩ when filled with internal solution, which consisted of 140 mM Cs-aspartate, 10 mM Cs_2-EGTA, 5 mM $MgCl_2$, and 10 mM HEPES, pH 7.4 with CsOH. The external recording solution contained 145 mM tetraethylammonium-Cl, 10 mM $CaCl_2$, 0.003 mM tetrodotoxin, and 10 mM HEPES, pH 7.4 with tetraethylammonium-OH. Linear capacitative and leakage currents were determined by averaging the currents elicited by eleven 30-mV hyperpolarizing pulses from a holding potential of −80 mV. Test currents were corrected for linear components of leak and capacitive current by digital scaling and subtraction of this average control current. Electronic compensation was used to reduce the effective series resistance (usually to <1 MΩ) and the time constant for charging the linear cell capacitance (usually to <0.5 ms). Ionic currents were filtered at 2–5 kHz and digitized at 10 kHz. To measure macroscopic L-type current in isolation, a 1 s prepulse to −20 mV followed by a 100 ms repolarization to −50 mV was administered before the test pulse (prepulse protocol; see Adams et al. (30)) to inactivate voltage-gated Na^+ and T-type Ca^{2+} channels. Cell capacitance was determined by integration of a transient from −80 to −70 mV using Clampex 8.0 (Molecular Devices, Sunnyvale, CA) and was used to normalize current amplitudes (pA/pF). *I/V* curves were fitted using the following equation:

$$I = G_{max} \times (V - V_{rev}) / \{1 + \exp[-(V - V_{1/2})/k_G]\}, \quad (1)$$

where I is the current for the test potential V, V_{rev} is the reversal potential, G_{max} is the maximum Ca^{2+} channel conductance, $V_{1/2}$ is the half-maximal activation potential, and k_G is the slope factor. The activation phase of L-type currents was fitted using the following exponential function:

$$I(t) = A_{fast}[\exp(-t/\tau_{fast})] + A_{slow}[\exp(-t/\tau_{slow})] + C, \quad (2)$$

where $I(t)$ is the current at time t after the depolarization, A_{fast} and A_{slow} are the steady-state current amplitudes of each component with their respective time constants of activation (τ_{fast} and τ_{slow}), and C represents the steady-state peak current (as in Avila and Dirksen (8)).

Tail current amplitude (I_{tail}) was measured 1 ms after the onset of the repolarization from the test pulse to −50 mV (31) and was used to calculate conductance via Ohm's law. In some experiments, L-type currents were recorded in the continuous presence of racemic Bay K 8644 (5 μM; kindly supplied by Dr. A. Scriabine, Miles Laboratories, Elkhart, IN) in the bath solution.

Measurement of charge movements

For measurement of intramembrane charge movements, ionic currents were blocked by the addition of 0.5 mM $CdCl_2$ + 0.1 mM $LaCl_3$ to the standard extracellular recording solution. All charge movements were measured with the prepulse protocol (see above) and were corrected for linear cell capacitance and leakage currents using a −P/6 subtraction protocol. Filtering was at 2–5 kHz (eight-pole Bessel filter; Frequency Devices, Ottawa, IL) and digitization was at 20 kHz. Voltage-clamp command pulses were exponentially rounded with a time constant of 50–500 μs. The integral of the ON transient (Q_{on}) for each test potential (V) was fitted according to

$$Q_{on} = Q_{max} / \{1 + \exp[-(V - V_Q)/k_Q]\}, \quad (3)$$

where Q_{max} is the maximal Q_{on}, V_Q is the potential causing movement of half the maximal charge, and k_Q is a slope parameter. For *dyspedic* myotubes, the normalized conductance (I_{tail}/Q_{max}) versus prior test potential (V) relationship was fitted according to

$$I_{tail}/Q_{max} = 1/\{1 + \exp[-(V - V_{tail})/k_{tail}]\}, \quad (4)$$

where V_{tail} is the potential causing half-maximal tail current and k_{tail} is a slope parameter.

Construction of RyR1-YFP

The plasmid containing RyR1-YFP was created in three steps using YFP-rabbit RyR1 (GenBank: X68650; a kind gift from Dr. M. Grabner) as a template. We first replaced the *Acc*65I restriction enzyme site at nucleotide 2,235 with a unique *Eco*RV site via a silent mutation (cgg tac c to cga tat c). This change was accomplished via a two-step, overlapping sequence PCR strategy with the primers designed to create a 1650 basepair product (5′ gctagcgctaccggtcgcc 3′ and reverse 5′ gccagatatcgtccggtgg 3′) and a separate 4084 basepair product (forward 5′ ggacgatatctggcactcacc 3′ and reverse 5′ ccatgccaccggttctcc 3′). These two PCR products were individually subcloned into separate TOPO PCR 2.1 vectors (Invitrogen, Carlsbad, CA). Both subcloned products were excised with *Age*I and *Eco*RV and ligated into an *Age*I-digested YFP-RyR1 via a three-piece ligation reaction. Next, we removed the carboxyl-terminal stop codon and inserted two nucleotide bases to this new, to our knowledge, *Eco*RV-modified YFP-RyR1 construct as a means to prevent the future carboxyl-terminal YFP from being out of frame. To do so, we used the forward primer 5′ ggtatactac ttcctggagg 3′ and the reverse primer 5′ gatcctctggtaccgctcagc 3′ to create a 1245-basepair product that was subsequently subcloned into TOPO PCR 2.1. The subcloned piece was then excised with *Bst*Z17I and *Acc*65I and ligated into a similarly cut *Eco*RV-modified YFP-RyR1 construct. Finally, the entire 15.1 kb modified RyR1 construct with *Eco*RV and ablated stop codon was excised with *Hin*dIII and *Acc*65I and ligated into a similarly cut YFP-N1 vector (Invitrogen) to produce the final RyR1-YFP product. The completed RyR1-YFP and all intermediate constructs were verified by sequencing at the DNA Sequencing and Analysis Core of the University of Colorado-Anschutz Medical Campus Cancer Center.

Analysis

Figures were made using the software program SigmaPlot (versions 7.0 and 11.0, Systat Software, San Jose, CA). All data are presented as mean ± SE. Statistical comparisons were by unpaired, two-tailed *t*-test or one-way analysis of variance (ANOVA) followed by a Dunnett's post hoc test (as appropriate), with $p < 0.05$ considered significant.

RESULTS

L-type current amplitude is greatly reduced in RyR1-E4242G myotubes

Fig. 1 *A* shows representative families of L-type currents recorded from normal and RyR1-E4242G myotubes. Typically, the density of L-type current recorded at the peak of the *I/V* relationship (+30 mV) from myotubes carrying the RyR1-E4242G mutation was reduced by ~80% in comparison to that of myotubes cultured from phenotypically normal littermates (−10.6 ± 0.9 pA/pF; $n = 21$ vs. −2.1 ± 0.1; $n = 53$, respectively; $p < 10^{-10}$, unpaired *t*-test; Fig. 1 B). Although there was a larger range in the individual current densities of normal (i.e., wild-type and heterozygous) myotubes relative to current densities of RyR1-E4242G myotubes, there was no overlap between the groups (R.A.B. and K.G.B., unpublished observation). A small depolarizing shift was observed in the activation phase of the curve ($V_{1/2}$ = 20.0 ± 1.3 mV and 24.1 ± 1.0 mV, for normal and RyR1-E4242G currents, respectively; $p < 0.05$, unpaired *t*-test; Table 1) and the reversal potential for RyR1-E4242G L-type current was routinely

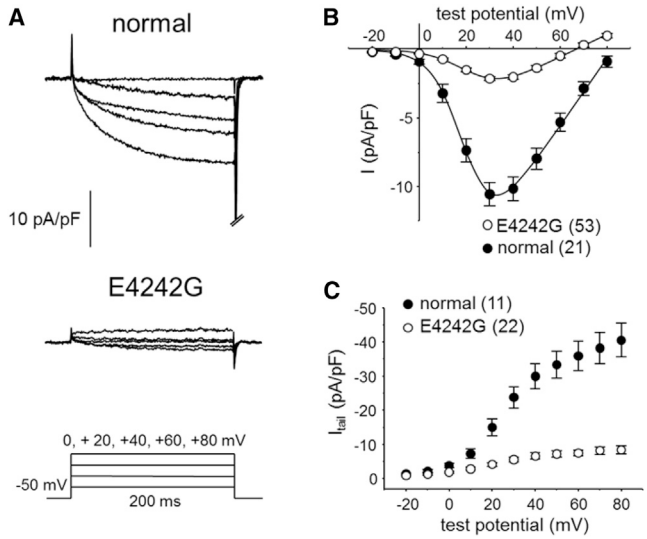

FIGURE 1 L-type currents are substantially reduced in RyR1-E4242G myotubes. (*A*) Representative families of L-type Ca^{2+} currents elicited by 200 ms depolarizations to the indicated test potentials are shown for a normal myotube (*top*) and an RyR1-E4242G myotube (*middle*). (*B*) Comparison of normal (●; $n = 21$) and RyR1-E4242G (○; $n = 53$) average peak *I/V* relationships. Currents were evoked at 0.1 Hz by test potentials ranging from −20 mV through +80 mV in 10 mV increments (illustrated at the *bottom* of *A*). Current amplitudes were normalized by linear cell capacitance (pA/pF). The smooth *I/V* curves are plotted according to Eq. 1. The best fit parameters for each plot are presented in Table 1. Throughout, error bars represent mean ± SE. (*C*) Comparison of normal (●; $n = 11$) and RyR1-E4242G (○; $n = 22$) I_{tail}/V relationships. I_{tail} was measured 1 ms after the onset of the repolarization from the indicated test pulse to −50 mV (31). The analysis tail current amplitude excluded cells with very small currents and cells in which tail current decay was obviously not monoexponential.

shifted by ~15 mV to more hyperpolarized potentials (Fig. 1, *B* and *C*). Such a shift in reversal potential is characteristic of low-amplitude L-type currents recorded from myotubes under similar experimental conditions (5,8,10,28) and likely arises from small outward leak currents. This being the case, a more accurate means of determining G_{max} was required, because an inaccurate reversal potential would distort the calculation of G_{max} via Eq. 1. Thus, tail current (I_{tail}) analysis was employed to quantify the effects of the RyR1-E4242G mutation on L-type channel gating. Tail current amplitude upon repolarization to −50 mV is plotted as a function of the test potential before repolarization in Fig. 1 *C*; the tail currents for RyR1-E4242G myotubes were substantially smaller (~80%) than those of normal myotubes. A good fit with a single Boltzmann expression was not possible for the I_{tail}/V relationship of either group because of the entry of $Ca_V1.1$ into mode 2 gating at stronger depolarizations (32–34). However, no obvious shift in the voltage-dependence of activation was apparent when the I_{tail}/V relationships were scaled to peak I_{tail} (Fig. S1 in the Supporting Material). Although the augmentation of L-type current amplitude by the 1,4-dihydropyridine agonist ±Bay K 8644 (5 μM) in

TABLE 1 Conductance and Intramembrane Charge Movement Fit Parameters

	G/V				*Q/V*		
Cell Type	G_{max} (nS/nF)	$V_{1/2}$ (mV)	k_G (mV)	V_{rev} (mV)	Q_{max} (nC/μF)	V_Q (mV)	k_Q (mV)
Normal	251 ± 2*** (21)	20.0 ± 1.3**	5.4 ± 0.2***	81.4 ± 1.6***	5.9 ± 0.7** (6)	−3.2 ± 3.9	8.1 ± 1.0
RyR1-E4242G	84 ± 6 (53)	24.1 ± 1.0	7.9 ± 0.4	67.0 ± 2.0	3.1 ± 0.5 (17)	1.7 ± 6.0	8.2 ± 1.7
RyR1-E4242G+ RyR1-YFP	119 ± 11 (13)	16.5 ± 2.3**	5.8 ± 0.4*	77.4 ± 2.6*		ND	
Dyspedic	44 ± 6** (15)	17.7 ± 1.9	8.7 ± 0.8	68.5 ± 4.2	3.7 ± 0.4 (10)	2.7 × 1.5	11.8 ± 1.0

I/V and *Q/V* curves are plotted according to Eqs. 1 and 3, respectively (see Materials and Methods). For all the data given, the calculated average voltage error was <5 mV. Data are given as mean ± SE, with the numbers in parentheses indicating the number of myotubes tested. Asterisks indicate significant differences compared to L-type currents or charge movements recorded from RyR1-E4242G myotubes (*$p < 0.05$; **$p < 0.01$; ***$p < 0.001$; one-way ANOVA followed by a Dunnett's post hoc test). ND, not determined.

RyR1-E4242G myotubes was not as substantial as the enhancement of the current in normal myotubes, RyR1-E4242G L-type currents still displayed slowed deactivation kinetics and hyperpolarizing shift in *I/V* relationship (R.A.B. and K.G.B., unpublished observation).

The RyR1-E4242G mutation results in reduced $Ca_V1.1$ expression and relative P_o

Intramembrane gating charge movements were measured to determine whether the decrease in L-type current density in RyR1-E4242G myotubes was simply a consequence of reduced $Ca_V1.1$ surface expression. The representative families of charge movements shown in Fig. 2, *A* and *B*, demonstrate that the RyR1-E4242G mutation does indeed decrease the number of $Ca_V1.1$ channels within the plasma membrane. On average, charge movement observed in normal myotubes (Q_{max} = 5.9 ± 0.7 nC/μF; n = 6) was nearly twice as large as that observed in RyR1-E4242G myotubes (Q_{max} = 3.1 ± 0.5 nC/μF; n = 17; $p < 0.01$; unpaired *t*-test; Fig. 2 *C*; Table 1). The reduction in Q_{max} for RyR1-E4242G myotubes indicates that decreased $Ca_V1.1$ expression was a consequence of the RyR1-E4242G mutation, presumably as a result of the loss of EC coupling (27), and is consistent with earlier work showing that Ca^{2+} flux via RyR1 regulates $Ca_V1.1$ expression levels (28).

Because RyR1-E4242G caused a reduced membrane density of $Ca_V1.1$, we divided I_{tail} (e.g., Fig. 3, *A* and *B*) at each test potential by the average value of Q_{max} to yield the relative channel open probability (P_o) as a function of test potential (Fig. 3 *C*). On the basis of these calculations, relative P_o in RyR1-E4242G myotubes was found to be reduced ~55% in comparison to that of normal myotubes (1.7 vs. 4.0 pA/fC, respectively, for repolarization from +30 to −50 mV). However, it is necessary to note that the measured Q_{max} did contain endogenous immobilization-resistant charge movement not attributable to $Ca_V1.1$ (Q_{dys}; (35)). Accordingly, the I_{tail}/Q_{max} values should be corrected by $Q_{max}/(Q_{max-}Q_{dys})$. If one assumes a Q_{dys} value of 1.0 nC/μF (36–38), a substantial, although reduced, difference in relative P_o remains between normal and RyR1-E4242G myotubes (4.8 vs. 2.6 pA/fC, respectively, for repolarization from +30 to −50 mV). Taken together, the combined ~50% reduction in expression and the ~55% reduction in P_o account for the observed ~80% L-type current reduction in RyR1-E4242G myotubes.

Importantly, I_{tail}/Q_{max} for RyR1-E4242G myotubes was larger than that of *dyspedic* myotubes (1.0 ± 0.2 pA/fC for repolarization from +30 mV to −50 mV; Fig. 3 *C*). Unlike the $I_{tail}/Q_{max}/V$ relationship for normal and RyR1-E4242G myotubes, the $I_{tail}/Q_{max}/V$ curve for *dyspedic* myotubes was fit well by a sigmoidal function, perhaps because there was a reduced entry into mode 2 gating. This result is consistent with the possibility that RyR1 plays a role in supporting the transition of $Ca_V1.1$ channels from mode 1 to mode 2 gating (39). In summary, the data presented in Figs. 2 and 3 indicate that RyR1s carrying the E4242G mutation were less effective in causing the retrograde increase in relative P_o compared to wild-type RyR1, and that the loss of EC coupling produced by the RyR1-E4242G mutation resulted in a reduced membrane expression of $Ca_V1.1$.

The retrograde effect of RyR1 on activation kinetics of the L-type current is little affected by the RyR1-E4242G mutation

The activation phase of L-type current in skeletal muscle can be best fit by the sum of two exponentials with time constants, τ_{fast} and τ_{slow}, and amplitudes A_{fast} and A_{slow} (Eq. 2; and see Avila and Dirksen (8)). In agreement with previous studies (8–10), both components of L-type current activation were visibly slower in normal (Fig. 4 *A*) than in *dyspedic* myotubes (Fig. 4 *B*). Surprisingly, L-type currents recorded from RyR1-E4242G myotubes (Fig. 4 *B*) retained the distinct slow activation characteristic of normal skeletal L-type currents (Fig. 4 *A*) and did not resemble the more rapid activation kinetics of *dyspedic* myotubes (Fig. 4 *C*). Quantitative analysis indicated that τ_{slow} and τ_{fast} for normal myotubes (92.3 ± 6.7 and 11.5 ± 1.9 ms, respectively; n = 14) and RyR1- E4242G myotubes (99.0 ± 11.2 and 13.8 ± 1.5 ms, respectively; n = 15) were not significantly different ($p > 0.05$, one-way ANOVA followed by a Dunnett's post hoc test; Table 2), whereas those for

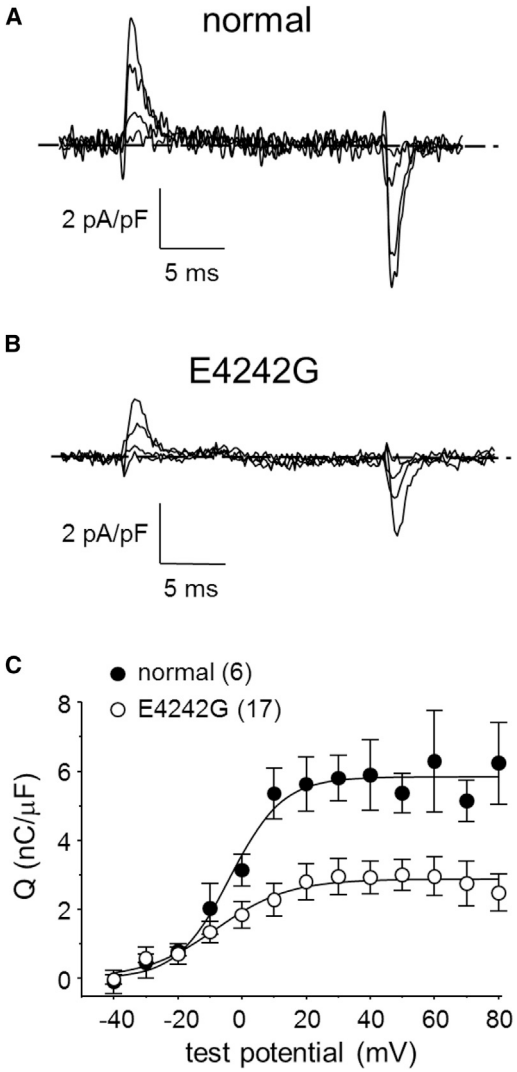

FIGURE 2 $Ca_V1.1$ expression is reduced in RyR1-E4242G myotubes. Charge movements elicited by 20 ms depolarizations from −50 to −30, −10, +10, and +30 mV are shown for a normal myotube (*A*) and an RyR1-E4242G myotube (*B*). (*C*) Comparison of normal (●; $n = 6$) and RyR1-E4242G (○; $n = 17$) Q/V relationships generated by 20 ms depolarizations from −50 mV to test potentials ranging from −40 mV through +80 mV in 10 mV increments. Only on-charges were analyzed because of the known ability of Cd^{2+} flux to contaminate the off-component. The smooth *Q/V* curves are plotted according to Eq. 3. The best fit parameters for each plot are presented in Table 1.

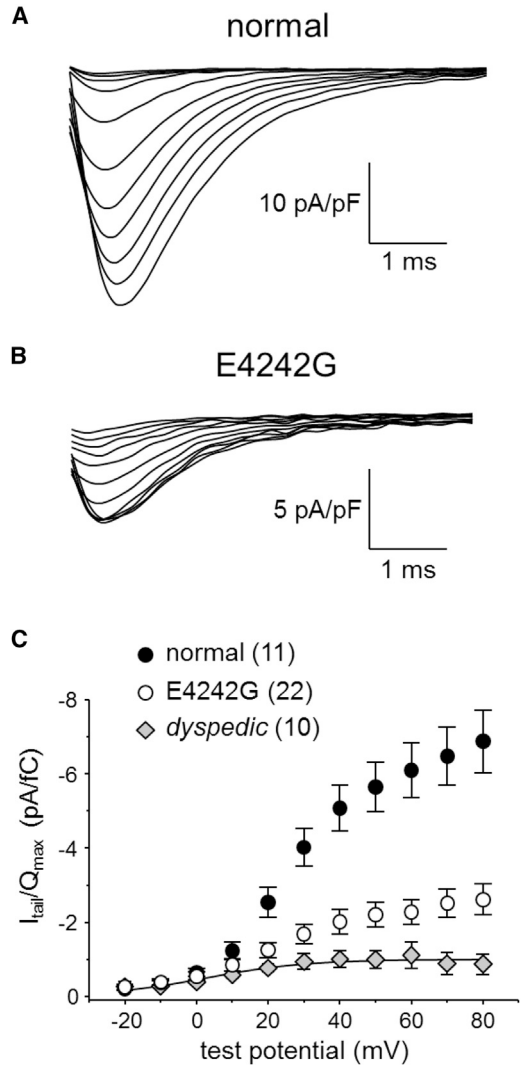

FIGURE 3 Relative P_o as a function of test potential. Representative families of tail currents elicited by repolarization to −50 mV after 200 ms test depolarizations (to −20 mV through +80 mV in 10 mV increments) are shown for a normal myotube (*A*) and a RyR1-E4242G myotube (*B*). Voltage protocol illustrated in Fig. 1 *A*, *bottom*. (*C*) Comparison of relative P_o (I_{tail}/Q_{max}) for normal (●; $n = 11$), RyR1-E4242G (○; $n = 22$), and *dyspedic* (◆; $n = 9$) P_o. The relative P_o values for *dyspedic* myotubes have been fit according to Eq. 4 with the following parameters: $I_{tail}/Q_{max} = 1.1 \pm 0.3$ pA/fC, $V_{tail} = 2.9 \pm 5.6$ mV, and $k_{tail} = 10.4 \pm 2.3$ mV. To obtain the measure of relative $Ca_V1.1$ P_o, conductance values (I_{tail}) have been divided by the respective average Q_{max} values for normal, RyR1-E4242G, and *dyspedic* myotubes (5.9, 3.1, and 3.7 nC/μF, respectively; see Table 1).

dyspedic myotubes were much faster (39.2 ± 10.0 and 3.3 ± 2.8 ms, respectively; $n = 8$; $p < 0.001$ and $p < 0.005$, respectively; Fig. 4 *D*; Table 2). The absolute values of A_{slow} and A_{fast} observed in normal myotubes (−9.5 ± 0.2 pA/pF and −1.5 × 0.2 pA/pF) were both considerably larger than those of RyR1-E4242G myotubes (−2.1 ± 0.3 pA/pF and −0.6 ± 0.1 pA/pF; both $p < 0.001$) and those of *dyspedic* myotubes (−0.6 ± 0.1 pA/pF and −0.3 ± 0.1 pA/pF; both $p < 0.001$; Fig. 4 *E*; Table 2). Although the relative contributions of A_{slow} and A_{fast} to the total current amplitude in normal (87 ± 1% and 13 ± 1%) myotubes was somewhat different than the fractional contributions in RyR1-E4242G (75 ± 4% and 25 ± 4%) and *dyspedic* (74 ± 7% and 26 ± 7%) myotubes, these differences were not significant (Table 2). The kinetic differences between *dyspedic* and RyR1-E4242G myotubes (i.e., τ_{fast} and τ_{slow}, absolute amplitudes of the respective components) presented in Fig. 4 indicate that resting interactions with the foot region of RyR1 are sufficient to slow channel activation (40).

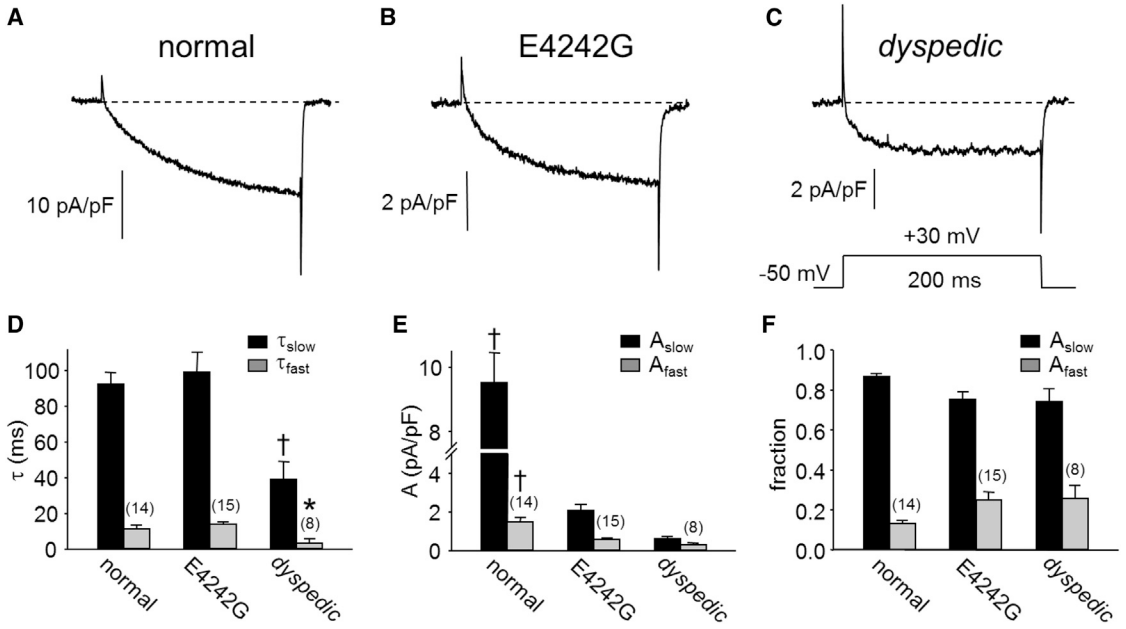

FIGURE 4 Comparison of activation kinetics of L-type current in normal, RyR1-E4242G and *dyspedic* myotubes. Representative macroscopic Ca^{2+} currents are shown for a normal myotube (*A*), a *dyspedic* myotube (*B*), and an RyR1-E4242G myotube (*C*). All currents analyzed were elicited by a 200 ms depolarization from −50 mV to +30 mV (illustrated in *C*). Activation was fitted with a double-exponential function (Eq. 2) yielding time constants τ_{fast} and τ_{slow} (*D*) with absolute (*E*) or fractional (*F*) amplitudes A_{fast} and A_{slow} (8). The best fit parameters for each group are presented in Table 2. Asterisks indicate significant differences (*$p < 0.005$; **$p < 0.001$) compared to RyR1-E4242G myotubes by one-way ANOVA followed by a Dunnett's post hoc test. The analysis of activation kinetics excluded cells with very small currents and cells in which tail current decay was obviously not monoexponential.

L-type current density in RyR1-E4242G myotubes is increased by exogenous expression of a wild-type RyR1-YFP fusion construct

We next sought to determine whether exogenous expression of wild-type RyR1 could completely rescue retrograde coupling. Fig. 5 *A* shows a family of L-type currents recorded from an RyR1-E4242G myotube expressing a wild-type RyR1-yellow fluorescent protein fusion construct (RyR1-YFP). These currents were substantially larger than any L-type current we measured in naive RyR1-E4242G myotubes (compare to Fig. 1 B). RyR1-E4242G myotubes expressing RyR1-YFP displayed a mean peak current density (−4.8 ± 0.5 pA/pF; $n = 13$; at +30 mV) that was significantly larger than that observed in naive RyR1-E4242G myotubes ($p < 0.001$; unpaired *t*-test; Fig. 5 *B*) or in naive *dyspedic* myotubes (−1.2 ± 0.1 pA/pF; $n = 15$; $p < 0.001$; unpaired *t*-test;). Although increased, the current density in RyR1-E4242G myotubes expressing RyR1-YFP was still considerably lower than in the normal myotubes.

DISCUSSION

In this study, we found that the RyR1-E4242G mutation has a profound effect on retrograde coupling between RyR1 and $Ca_V1.1$ in skeletal muscle. L-type currents recorded from homozygous RyR1-E4242G myotubes were reduced ~80% in comparison to those of phenotypically normal littermates (Fig. 1). The reduction in peak current amplitude was found to be the result of both a decrease in $Ca_V1.1$ plasma membrane expression and relative $Ca_V1.1$ P_o (Figs. 2 and 3, respectively). The disruption of retrograde coupling in RyR1-E4242G myotubes resembled the loss of retrograde coupling in *dyspedic* (RyR1 null) myotubes

TABLE 2 Activation Fit Parameters

	A_{slow}			A_{fast}		
	τ_{slow} (ms)	A_{slow} (pA/pF)	Fraction (%)	τ_{fast} (ms)	A_{fast} (pA/pF)	Fraction (%)
Normal	92.3 ± 6.7 (14)	9.5 ± 0.2**	87 ± 1	11.5 ± 1.9	1.5 ± 0.2**	13 ± 1
RyR1-E4242G	99.0 ± 11.2 (15)	2.1 ± 0.3	75 ± 4	13.8 ± 1.5	0.6 ± 0.1	25 ± 4
dyspedic	39.2 ± 10.0** (8)	0.6 ± 0.1	74 ± 7	3.3 ± 2.8*	0.3 ± 0.1	26 ± 7

All currents analyzed were elicited by a 200 ms depolarization from −50 mV to +30 mV after a prepulse protocol (see Materials and Methods). Activation was fitted with a double-exponential function yielding time constants τ_{fast} and τ_{slow} with absolute or fractional amplitudes A_{fast} and A_{slow} (Eq. 2; see Avila and Dirksen (8)). Data are given as mean ± SE, with the numbers in parentheses indicating the number of myotubes tested. Asterisks indicate significant differences relative to RyR1-E4242G myotubes (*$p < 0.005$; **$p < 0.001$; as determined by one-way ANOVA followed by a Dunnett's post hoc test).

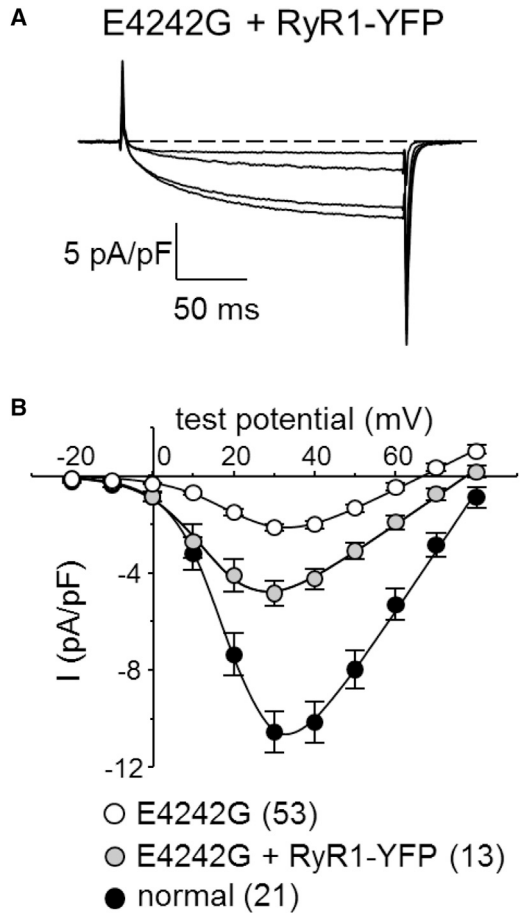

FIGURE 5 Retrograde coupling in RyR1-E4242G myotubes is partially restored by exogenous expression of a wild-type RyR1-YFP fusion construct. (*A*) Representative family of L-type currents elicited by the voltage protocol described in Fig. 1 A (*bottom*) are shown for an RyR1-E4242G myotube expressing RyR1-YFP. (*B*) *I/V* relationships for RyR1-E4242G myotubes expressing RyR1-YFP (●; $n = 13$). *I/V* curves for normal myotubes (●) and naive RyR1-E4242G myotubes (○) are replotted from Fig. 1 *B* for comparison. The best fit parameters for each plot are presented in Table 1.

with one key exception—the activation kinetics of RyR1-E4242G L-type current mirrored the slow activation kinetics of normal L-type currents, rather than the rapidly activating L-type currents of *dyspedic* myotubes (Fig. 4). The retention of wild-type current activation kinetics indicated that the mutated RyR1 was capable of partial retrograde communication with $Ca_V1.1$. Exogenous expression of a wild-type RyR1 construct restored L-type current density to ~45% of normal myotubes (Fig. 5).

The first conclusion that can be made based on these observations is that the side chain of RyR1 residue E4242 is critical for complete retrograde coupling between these ion channels. The importance of this residue for RyR1 function is underscored by its conservation among mice, rats, rabbits, and humans. It is unlikely, however, that this residue represents a locus of physical interaction between the RyR1 and $Ca_V1.1$ (or an intermediary protein) as cryo-EM images of RyR1 indicate that E4242 resides near the interface between the myoplasmic foot domain and the sarcoplasmic reticulum membrane-bound pore region of RyR1 (41–43). These images of RyR1 suggest that a residue in this position would be buried beneath the bulk of the foot region, ~12 nm away from the voltage-sensing domains of $Ca_V1.1$. For these reasons, we think it is more likely that the E4242G mutation alters conformations of RyR1 that support bidirectional communication with $Ca_V1.1$. The second conclusion is that two or more interactions between RyR1 and $Ca_V1.1$ are involved in retrograde signaling, and these two interactions are at least partially independent of one another.

Our results enable us to refine the model of bidirectional coupling between RyR1 and $Ca_V1.1$ that was first proposed by Nakai et al. (5) and expanded by Avila and Dirksen (8). This model (Fig. 6) illustrates three signaling interactions between $Ca_V1.1$ and RyR1: an orthograde EC coupling signal and two separate retrograde signals. The orthograde EC coupling signal is severely impaired by the RyR1-E4242G mutation (27), as is the retrograde enhancement

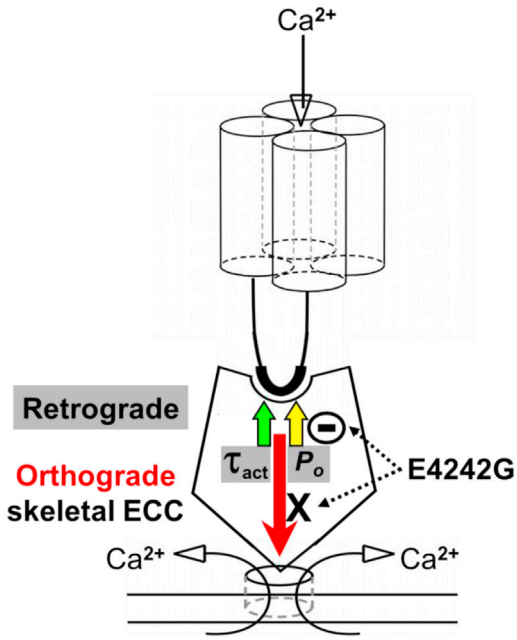

FIGURE 6 Schematic diagram of bidirectional coupling between RyR1 and $Ca_V1.1$ and the effects of the RyR1-E4242G mutation on this coupling. The red arrow represents the orthograde signal between RyR1 and $Ca_V1.1$. The smaller green and yellow arrows represent the two components of retrograde coupling (slowed activation kinetics and enhanced channel P_o, respectively). This model has been modified from a previous model (5) in which these two separable components of retrograde signaling were considered to be inherently united and were represented by a single arrow. For simplicity, a direct coupling between $Ca_V1.1$ and RyR1 is shown even though such a direct coupling mechanism has not been confirmed (13). Structural data seem to indicate that RyR1 residue E4242 is not involved in direct interactions with the $Ca_V1.1$ channel complex or any other intermediates that link the two channels (41–43). The model presented here is consistent with the view that multiple loci of interaction between RyR1 and $Ca_V1.1$ support efficient EC coupling in skeletal muscle (for a review, please see Beam and Bannister (44)). To see this figure in color, go online.

of $Ca_V1.1$ P_o (Fig. 3 *C*). However, the slowing of $Ca_V1.1$ activation kinetics is unaffected by the RyR1-E4242G mutation. The two, retrograde modulatory effects of wild-type RyR1 on the L-type current can be thought of as similar to those of other auxiliary subunits of voltage-gated Ca^{2+} channels (45). For example, $Ca_V\beta$ subunits affect both P_o and kinetics of high-voltage-activated Ca^{2+} channels (for a review, please see Buraei and Yang (46)). Suggestive evidence in support of the idea that RyR1 behaves like a cytoplasmic subunit is provided by a previous study, which demonstrated by means of fluorescence resonance energy transfer that RyR1 causes rearrangement of the cytoplasmic domains of $Ca_V1.1$ (47). Our present results indicate that these components of retrograde coupling are separable and therefore dependent on distinct structural elements within RyR1.

Previous work has shown that in addition to causing increased relative P_o and slowed activation of the L-type current, RyR1 also increases membrane expression of $Ca_V1.1$, as indicated by Q_{max} (28). This latter effect depends upon EC coupling Ca^{2+} release, which does not occur for RyR1-E4242G. However, the relative P_o should be unaffected by any changes in $Ca_V1.1$ membrane expression because our estimate of relative P_o was obtained by calculating the ratio between I_{tail} and Q_{max}. In regard to the slowed L-type current activation caused by RyR1-E4242G, it is interesting to note that previous work with normal myotubes showed that activation was slower in cells with lower $Ca_V1.1$ expression (48). However, we do not think that this effect can account for the effect of RyR1-E4242G on activation because Q_{max} was not significantly different between *dyspedic* myotubes and RyR1-E4242G myotubes (Table 1).

As mentioned above, the model shown in Fig. 6 indicates that EC coupling is severely impaired by RyR1-E4242G, which is based on our observations that were included in Fig. 2 of Hanson and Niswander (27). In that work, it was also shown that electromyographic (EMG) activity was absent in directly stimulated diaphragms of E18.5 mice homozygous for RyR1-E4242G, but restored by raising extracellular K^+ from 3 to 6 mM. This effect cannot be attributed to enhanced EC coupling because the EMG is an event occurring upstream from activation of RyR1 (wild-type or mutant) by $Ca_V1.1$. It was also reported that contractility (Fig. 3H of Hanson and Niswander (27)) was increased from zero in E18.5 diaphragms of RyR1-E4242G homozygotes to one in such diaphragms exposed to elevated K^+, the K_{ATP} channel blocker glibencamide (2 μM) or Bay K 8644 (100 nM), where a contractility of one was defined as either the presence of an EMG response or a visual observation of movement. From these results, it cannot be determined whether the movements were weak or strong and whether they resulted from skeletal-type EC coupling or another mechanism (e.g., Ca^{2+} flux via $Ca_V1.1$).

L-type Ca^{2+} channels appear to have two open gating modes, one of which (mode 1) is characterized by brief openings and the other (mode 2) by longer-lasting openings (32); transitions from mode 1 to mode 2 are promoted by stronger and longer-lasting depolarizations (33). The progression of channels from mode 1 to mode 2 is reflected macroscopically upon repolarization by tail currents that are larger and more slowly decaying, and can account for the observation that tail currents of wild-type and RyR1-E4242G myotubes display an initial steep increase for modest depolarizations followed by a shallower, but ongoing, growth in amplitude for stronger depolarizations (Fig. 3). RyR1 appeared to affect both components for $Ca_V1.1$. Specifically, RyR1 appeared to increase the likelihood of mode 1 openings inasmuch as it increased the amplitudes of tail currents for modest prior depolarizations ($\leq$20 mV) compared to those in *dyspedic* myotubes (Fig. 3). RyR1 also appeared to promote the entry of $Ca_V1.1$ into mode 2 openings. Thus, the tail currents of *dyspedic* myotubes obeyed a saturating Boltzmann dependence on prior test potential (Fig. 3), as if entry into mode 2 does not occur without RyR1 present. Consistent with the idea that the presence of RyR1 promotes entry into mode 2, and that entry into mode 2 does not occur without RyR1, Fleig et al. (39) found that, compared to 50 ms depolarizations to +80 mV, 600 ms depolarizations evoked larger, more slowly decaying tail currents in normal myotubes, whereas such tail current enhancement was absent in *dyspedic* myotubes.

We postulate that the partial restoration of L-type current amplitude in RyR1-E4242G myotubes by reintroduction of wild-type RyR1 (Fig. 4) was most likely a consequence of increasing the number of junctional RyR1s that are fully functional with regard to bidirectional signaling. Additionally, restoration of EC coupling likely increased expression of $Ca_V1.1$ (28). Still, further work is required to determine whether the trafficking and assembly of RyR1s is adversely affected by the E4242G mutation, and to determine the relative expression of the wild-type and mutant alleles in mice heterozygous for RyR1-E4242G. This information is needed to fully understand how heteromers of wild-type RyR1 and RyR1-E4242G affect both orthograde and retrograde coupling.

Although the physiological significance of Ca^{2+} flux via $Ca_V1.1$ has been the subject of much debate since the 1960s, recent work has revealed that L-type Ca^{2+} entry maintains myoplasmic Ca^{2+} levels during repetitive activity (49–51), augments muscle contraction (52), engages excitation-transcription coupling (51), and promotes formation of neuromuscular junctions during development (53–55). Moreover, conformational coupling between RyR1 and L-type Ca^{2+} channels has been shown to trigger transient elevations in cytoplasmic Ca^{2+} in neurons (56–60). Taken together, these findings highlight the importance of exploring the nature of $Ca_V1.1$-RyR1 conformational

coupling, as it is clear that this interaction forms the mechanistic basis for the generation of some localized Ca^{2+} signals in neurons, as well as those required for EC coupling in skeletal muscle.

SUPPORTING MATERIAL

One figure is available at http://www.biophysj.org/biophysj/supplemental/S0006-3495(16)00004-7.

AUTHOR CONTRIBUTIONS

R.A.B. designed research, performed research, analyzed data, and wrote the article; K.G.B. designed research, analyzed data, and wrote the article; and D.C.S. performed research and provided unique research materials. All authors read and approved the final article.

ACKNOWLEDGMENTS

We thank Dr. J.D. Ohrtman and Ms. O. Moua for their assistance during the course of the project. We also are grateful to Dr. M. Grabner for the gift of the RyR1 parent construct. RyR1-E4242G mice and phenotypically normal littermates were provided by Dr. L.A. Niswander (Department of Paediatrics, University of Colorado School of Medicine).

This work was supported in part by grants from the National Institutes of Health (2P01 AR052354 and AR055104 to K.G.B. and AG038778 to R.A.B.). R.A.B. was supported by a developmental grant from the Muscular Dystrophy Association (No. MDA4155). D.C.S. was supported by a National Institutes of Health training grant (No. NS543115-04) and a developmental grant (No. MDA4334) from the Muscular Dystrophy Association.

REFERENCES

1. Schneider, M. F., and W. K. Chandler. 1973. Voltage dependent charge movement of skeletal muscle: a possible step in excitation-contraction coupling. *Nature.* 242:244–246.
2. Ríos, E., and G. Brum. 1987. Involvement of dihydropyridine receptors in excitation-contraction coupling in skeletal muscle. *Nature.* 325:717–720.
3. Tanabe, T., K. G. Beam, …, S. Numa. 1988. Restoration of excitation-contraction coupling and slow calcium current in dysgenic muscle by dihydropyridine receptor complementary DNA. *Nature.* 336:134–139.
4. Bannister, R. A., and K. G. Beam. 2013. $Ca_V1.1$: the atypical prototypical voltage-gated Ca^{2+} channel. *Biochim. Biophys. Acta.* 1828:1587–1597.
5. Nakai, J., R. T. Dirksen, …, P. D. Allen. 1996. Enhanced dihydropyridine receptor channel activity in the presence of ryanodine receptor. *Nature.* 380:72–75.
6. Nakai, J., N. Sekiguchi, …, K. G. Beam. 1998. Two regions of the ryanodine receptor involved in coupling with L-type Ca^{2+} channels. *J. Biol. Chem.* 273:13403–13406.
7. Grabner, M., R. T. Dirksen, …, K. G. Beam. 1999. The II-III loop of the skeletal muscle dihydropyridine receptor is responsible for the bidirectional coupling with the ryanodine receptor. *J. Biol. Chem.* 274:21913–21919.
8. Avila, G., and R. T. Dirksen. 2000. Functional impact of the ryanodine receptor on the skeletal muscle L-type Ca^{2+} channel. *J. Gen. Physiol.* 115:467–480.
9. Ahern, C. A., D. C. Sheridan, …, R. Coronado. 2003. Ca^{2+} current and charge movements in skeletal myotubes promoted by the β-subunit of the dihydropyridine receptor in the absence of ryanodine receptor type 1. *Biophys. J.* 84:942–959.
10. Sheridan, D. C., H. Takekura, …, C. F. Perez. 2006. Bidirectional signaling between calcium channels of skeletal muscle requires multiple direct and indirect interactions. *Proc. Natl. Acad. Sci. USA.* 103:19760–19765.
11. Balog, E. M., and E. M. Gallant. 1999. Modulation of the sarcolemmal L-type current by alteration in SR Ca^{2+} release. *Am. J. Physiol.* 276:C128–C135.
12. Bannister, R. A., and K. G. Beam. 2009. Ryanodine modification of RyR1 retrogradely affects L-type Ca^{2+} channel gating in skeletal muscle. *J. Muscle Res. Cell Motil.* 30:217–223.
13. Bannister, R. A. 2015. Bridging the myoplasmic gap II: more recent advances in skeletal muscle excitation-contraction coupling. *J. Exp. Biol.*, In press.
14. Tanabe, T., K. G. Beam, …, S. Numa. 1990. Regions of the skeletal muscle dihydropyridine receptor critical for excitation-contraction coupling. *Nature.* 346:567–569.
15. Nakai, J., T. Tanabe, …, K. G. Beam. 1998. Localization in the II-III loop of the dihydropyridine receptor of a sequence critical for excitation-contraction coupling. *J. Biol. Chem.* 273:24983–24986.
16. Beurg, M., C. A. Ahern, …, R. Coronado. 1999. Involvement of the carboxy-terminus region of the dihydropyridine receptor β_{1a} subunit in excitation-contraction coupling of skeletal muscle. *Biophys. J.* 77:2953–2967.
17. Sheridan, D. C., W. Cheng, …, R. Coronado. 2004. Involvement of a heptad repeat in the carboxyl terminus of the dihydropyridine receptor β_{1a} subunit in the mechanism of excitation-contraction coupling in skeletal muscle. *Biophys. J.* 87:929–942.
18. Rebbeck, R. T., Y. Karunasekara, …, A. F. Dulhunty. 2011. The $\beta(_{1a})$ subunit of the skeletal DHPR binds to skeletal RyR1 and activates the channel via its 35-residue C-terminal tail. *Biophys. J.* 100:922–930.
19. Leong, P., and D. H. MacLennan. 1998. A 37-amino acid sequence in the skeletal muscle ryanodine receptor interacts with the cytoplasmic loop between domains II and III in the skeletal muscle dihydropyridine receptor. *J. Biol. Chem.* 273:7791–7794.
20. Leong, P., and D. H. MacLennan. 1998. The cytoplasmic loops between domains II and III and domains III and IV in the skeletal muscle dihydropyridine receptor bind to a contiguous site in the skeletal muscle ryanodine receptor. *J. Biol. Chem.* 273:29958–29964.
21. Sencer, S., R. V. Papineni, …, S. L. Hamilton. 2001. Coupling of RYR1 and L-type calcium channels via calmodulin binding domains. *J. Biol. Chem.* 276:38237–38241.
22. Cheng, W., X. Altafaj, …, R. Coronado. 2005. Interaction between the dihydropyridine receptor Ca^{2+} channel β-subunit and ryanodine receptor type 1 strengthens excitation-contraction coupling. *Proc. Natl. Acad. Sci. USA.* 102:19225–19230.
23. Proenza, C., J. J. O'Brien, …, K. G. Beam. 2002. Identification of a region of RyR1 that participates in allosteric coupling with the α_{1S} ($Ca_V1.1$) II–III loop. *J. Biol. Chem.* 277:6530–6535.
24. Protasi, F., C. Paolini, …, P. D. Allen. 2002. Multiple regions of RyR1 mediate functional and structural interactions with $\alpha(_{1S})$-dihydropyridine receptors in skeletal muscle. *Biophys. J.* 83:3230–3244.
25. Perez, C. F., S. Mukherjee, and P. D. Allen. 2003. Amino acids 1–1,680 of ryanodine receptor type 1 hold critical determinants of skeletal type for excitation-contraction coupling. Role of divergence domain D2. *J. Biol. Chem.* 278:39644–39652.
26. Perez, C. F., A. Voss, …, P. D. Allen. 2003. RyR1/RyR3 chimeras reveal that multiple domains of RyR1 are involved in skeletal-type E-C coupling. *Biophys. J.* 84:2655–2663.
27. Gartz Hanson, M., and L. A. Niswander. 2015. Rectification of muscle and nerve deficits in paralyzed ryanodine receptor type 1 mutant embryos. *Dev. Biol.* 404:76–87.
28. Avila, G., K. M. S. O'Connell, …, R. T. Dirksen. 2001. Ca^{2+} release through ryanodine receptors regulates skeletal muscle L-type Ca^{2+} channel expression. *J. Biol. Chem.* 276:17732–17738.

29. Beam, K. G., and C. Franzini-Armstrong. 1997. Functional and structural approaches to the study of excitation-contraction coupling. *Methods Cell Biol.* 52:283–306.
30. Adams, B. A., T. Tanabe, …, K. G. Beam. 1990. Intramembrane charge movement restored in dysgenic skeletal muscle by injection of dihydropyridine receptor cDNAs. *Nature.* 346:569–572.
31. Wilkens, C. M., M. Grabner, and K. G. Beam. 2001. Potentiation of the cardiac L-type Ca^{2+} channel (α(1C)) by dihydropyridine agonists and strong depolarization occur via distinct mechanisms. *J. Gen. Physiol.* 118:495–508.
32. Hess, P., J. B. Lansman, and R. W. Tsien. 1984. Different modes of Ca channel gating behaviour favoured by dihydropyridine Ca agonists and antagonists. *Nature.* 311:538–544.
33. Pietrobon, D., and P. Hess. 1990. Novel mechanism of voltage-dependent gating in L-type calcium channels. *Nature.* 346:651–655.
34. Bannister, R. A., and K. G. Beam. 2013. Impaired gating of an L-type Ca^{2+} channel carrying a mutation linked to malignant hyperthermia. *Biophys. J.* 104:1917–1922.
35. Adams, B. A., and K. G. Beam. 1989. A novel calcium current in dysgenic skeletal muscle. *J. Gen. Physiol.* 94:429–444.
36. Bannister, R. A., and K. G. Beam. 2005. The α_{1S} N-terminus is not essential for bi-directional coupling with RyR1. *Biochem. Biophys. Res. Commun.* 336:134–141.
37. Bannister, R. A., M. Grabner, and K. G. Beam. 2008. The α_{1S} III–IV loop influences DHPR gating but is not directly involved in excitation-contraction coupling interactions with the type 1 ryanodine receptor. *J. Biol. Chem.* 283:23217–23223.
38. Bannister, R. A., S. Papadopoulos, …, K. G. Beam. 2009. Effects of inserting fluorescent proteins into the α_{1S} II-III loop: insights into excitation-contraction coupling. *J. Gen. Physiol.* 134:35–51.
39. Fleig, A., H. Takeshima, and R. Penner. 1996. Absence of Ca^{2+} current facilitation in skeletal muscle of transgenic mice lacking the type 1 ryanodine receptor. *J. Physiol.* 496:339–345.
40. Hurne, A. M., J. J. O'Brien, …, I. N. Pessah. 2005. Ryanodine receptor type 1 (RyR1) mutations C4958S and C4961S reveal excitation-coupled calcium entry (ECCE) is independent of SR store depletion. *J. Biol. Chem.* 280:36994–37004.
41. Efremov, R. G., A. Leitner, …, S. Raunser. 2015. Architecture and conformational switch mechanism of the ryanodine receptor. *Nature.* 517:39–43.
42. Yan, Z., X. C. Bai, …, N. Yan. 2015. Structure of the rabbit ryanodine receptor RyR1 at near-atomic resolution. *Nature.* 517:50–55.
43. Zalk, R., O. B. Clarke, …, A. R. Marks. 2015. Structure of a mammalian ryanodine receptor. *Nature.* 517:44–49.
44. Beam, K. G., and R. A. Bannister. 2010. Looking for answers to EC coupling's persistent questions. *J. Gen. Physiol.* 136:7–12.
45. Campiglio, M., and B. E. Flucher. 2015. The role of auxiliary subunits for the functional diversity of voltage-gated calcium channels. *J. Cell. Physiol.* 230:2019–2031.
46. Buraei, Z., and J. Yang. 2010. The β subunit of voltage-gated Ca^{2+} channels. *Physiol. Rev.* 90:1461–1506.
47. Polster, A., J. D. Ohrtman, …, S. Papadopoulos. 2012. Fluorescence resonance energy transfer (FRET) indicates that association with the type I ryanodine receptor (RyR1) causes reorientation of multiple cytoplasmic domains of the dihydropyridine receptor (DHPR) $\alpha_{(1S)}$ subunit. *J. Biol. Chem.* 287:41560–41568.
48. Adams, B. A., T. Tanabe, and K. G. Beam. 1996. Ca^{2+} current activation rate correlates with α_1 subunit density. *Biophys. J.* 71:156–162.
49. Cherednichenko, G., A. M. Hurne, …, I. N. Pessah. 2004. Conformational activation of Ca^{2+} entry by depolarization of skeletal myotubes. *Proc. Natl. Acad. Sci. USA.* 101:15793–15798.
50. Bannister, R. A., I. N. Pessah, and K. G. Beam. 2009. The skeletal L-type Ca^{2+} current is a major contributor to excitation-coupled Ca^{2+} entry. *J. Gen. Physiol.* 133:79–91.
51. Lee, C. S., A. Dagnino-Acosta, …, S. L. Hamilton. 2015. Ca^{2+} permeation and/or binding to $Ca_V1.1$ fine-tunes skeletal muscle Ca^{2+} signaling to sustain muscle function. *Skelet. Muscle.* 5:4.
52. Mosca, B., O. Delbono, …, F. Zorzato. 2013. Enhanced dihydropyridine receptor calcium channel activity restores muscle strength in JP45/CASQ1 double knockout mice. *Nat. Commun.* 4:1541.
53. Caroni, P., S. Rotzler, …, H. R. Brenner. 1993. Calcium influx and protein phosphorylation mediate the metabolic stabilization of synaptic acetylcholine receptors in muscle. *J. Neurosci.* 13:1315–1325.
54. Chen, F., Y. Liu, …, W. Lin. 2011. Neuromuscular synaptic patterning requires the function of skeletal muscle dihydropyridine receptors. *Nat. Neurosci.* 14:570–577.
55. Flucher, B. E., and P. Tuluc. 2011. A new L-type calcium channel isoform required for normal patterning of the developing neuromuscular junction. *Channels (Austin).* 5:518–524.
56. Chavis, P., L. Fagni, …, J. Bockaert. 1996. Functional coupling between ryanodine receptors and L-type calcium channels in neurons. *Nature.* 382:719–722.
57. Ouardouz, M., M. A. Nikolaeva, …, P. K. Stys. 2003. Depolarization-induced Ca^{2+} release in ischemic spinal cord white matter involves L-type Ca^{2+} channel activation of ryanodine receptors. *Neuron.* 40:53–63.
58. De Crescenzo, V., K. E. Fogarty, …, J. V. Walsh, Jr. 2006. Dihydropyridine receptors and type 1 ryanodine receptors constitute the molecular machinery for voltage-induced Ca^{2+} release in nerve terminals. *J. Neurosci.* 26:7565–7574.
59. Kim, S., H. M. Yun, …, H. Rhim. 2007. Functional interaction of neuronal $Ca_v1.3$ L-type calcium channel with ryanodine receptor type 2 in the rat hippocampus. *J. Biol. Chem.* 282:32877–32889.
60. De Crescenzo, V., K. E. Fogarty, …, J. V. Walsh, Jr. 2012. Type 1 ryanodine receptor knock-in mutation causing central core disease of skeletal muscle also displays a neuronal phenotype. *Proc. Natl. Acad. Sci. USA.* 109:610–615.